Velocity field for Taylor–Couette flow with an axial flow

Steven T. Wereley[a] and Richard M. Lueptow[b]
Department of Mechanical Engineering, Northwestern University, 2145 Sheridan Road, Evanston, Illinois 60208

(Received 3 November 1998; accepted 18 August 1999)

The flow in the gap between an inner rotating cylinder concentric with an outer stationary cylinder with an imposed pressure-driven axial flow was studied experimentally using particle image velocimetry (PIV) in a meridional plane of the annulus. The radius ratio was $\eta = 0.83$ and the aspect ratio was $\Gamma = 47$. Velocity vector fields for nonwavy toroidal and helical vortices show the axial flow winding around vortices. When the axially averaged axial velocity profile is removed from the velocity field in a meridional plane, the velocity field looks much like it would with no imposed axial flow except that the vortices translate axially and the distortion of the azimuthal velocity contours in meridional plane related to the vortices is shifted axially by the axial flow. The velocity vector fields for wavy vortices also show axial flow winding around the vortices. Again, removing the axial velocity profile results in a flow that appears similar to that with no axial flow. The path of the vortices is generally axial, but the vortices periodically move retrograde to the imposed axial flow due to the waviness of the vortices. The axial velocity of helical vortices, both nonwavy and wavy, is twice the rotational frequency of the inner cylinder indicating a coupling between the axial translation of the vortices and the cylinder rotation. Little fluid transport between vortices occurs for nonwavy vortices, but there is substantial transport between vortices for wavy vortex flow, much like supercritical cylindrical Couette flow with no axial flow. © *1999 American Institute of Physics.* [S1070-6631(99)01412-9]

I. INTRODUCTION

Pressure-driven axial flow in an annulus between a rotating inner cylinder and a fixed outer cylinder has several important engineering applications including journal bearings, biological separation devices, and rotating machinery. A centrifugal instability related to the curved streamlines of the flow results in toroidal Taylor vortices in the annulus. Taylor's linear stability analysis for cylindrical Couette flow[1] can readily be extended to include an axial flow in the annulus for axisymmetric disturbances in a narrow annular gap[2–4] or an arbitrarily wide annular gap.[5,6] At transition to supercritical flow, the flow consists of toroidal Taylor vortices translating with the imposed axial flow at a theoretical velocity of about 1.2 times the mean velocity of the axial flow.[6–8] Nonaxisymmetric analysis predicts pairs of helical vortices with an inclination opposite that of the base flow for axial Reynolds numbers above a critical value.[7,9,10] Experimental results confirm the appearance of translating toroidal vortices at low Reynolds numbers and helical vortices at higher Reynolds numbers.[10–13] The axial flow stabilizes the cylindrical Couette flow such that transition to Taylor vortex flow occurs at a higher Taylor number than with no axial flow.[11,12,14–16] Recently, cylindrical Couette flow with an imposed axial flow has been used to compare absolutely and convectively unstable regimes.[8,17–20]

The research described above focused on the first instability transition from stable Couette–Poiseuille flow to translating toroidal or helical vortex flow. Higher order instability transitions have been mapped out in the Taylor number-Reynolds number plane. Early work differentiated only two unstable flow regimes beyond stable Couette–Poiseuille flow and Taylor vortex flow: turbulent Taylor vortices and fully turbulent flow with no vortices.[21–23] More recent experiments identified a rich variety of flow regimes including translating wavy vortices, translating helical wavy vortices, turbulent wavy vortices, and vortices with random waviness.[24–29] Other recent experiments have considered the mass transfer character in Couette–Poiseuille flow.[13]

Although the stability of the flow and the variety of flow regimes for cylindrical Couette flow with an imposed axial flow have been studied in depth, the velocity field has not been studied in detail. Limited hot-wire and laser Doppler velocimetry (LDV) measurements of the time-averaged axial and azimuthal velocities at high axial Reynolds numbers indicate that the azimuthal velocity profile has very steep gradients near both walls of the annulus.[30–32] The ratio of the Taylor number to the axial Reynolds number, representing the ratio of centrifugal to advective accelerations, has been used to characterize the flow.[31,33] When the ratio is large, the vortices are strong and their effect is readily apparent in the velocity field. When this ratio is small, the dominant axial velocity overwhelms the supercritical vortices resulting in fluid winding around small vortices that are alternatively close to the inner and outer walls.

The aim of the present work is to examine the velocity

[a]Present address: School of Mechanical Engineering, Purdue University, West Lafayette, IN.
[b]Author to whom correspondence should be addressed: Telephone: 847-491-4265; Fax: 847-491-3915; Electronic mail: r-lueptow@nwu.edu

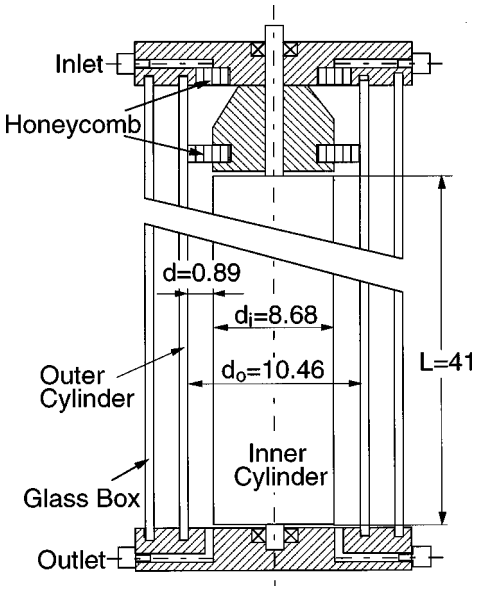

FIG. 1. Sketch of the experimental apparatus. Dimensions are in cm.

field for cylindrical Couette flow with an imposed axial flow. We are particularly interested in the axial translation of vortices, the properties of the flow states, and the details of the fluid transport between vortices. Unlike the previous time-averaged, single point hot-wire and LDV measurements for this flow,[30–32] we used PIV to provide time-resolved measurements of the radial and axial velocity in a meridional plane of the flow. Furthermore, our measurements included axisymmetric and nonaxisymmetric (wavy or helical) vortex regimes, whereas previous computational work was purely axisymmetric.[33]

II. EXPERIMENTAL APPARATUS AND PROCEDURE

The flow system consisted of two concentric cylinders, an inner rotating acrylic cylinder and an outer glass cylinder with diameters $2r_i = 8.680 \pm 0.003$ cm and $2r_o = 10.46 \pm 0.03$ cm, respectively, as shown in Fig. 1. The resulting gap width was $d = r_o - r_i = 0.89$ cm, and the radius ratio was $\eta = r_i / r_o = 0.83$. The inner cylinder was driven by a stepper motor allowing computer control of the rotational speed of the inner cylinder to better than 0.1%. The two cylinders were held concentric by aluminum endcaps. The ratio of the length of the annulus to the gap width was $\Gamma = 46.6$. The working fluid flowed from an upper constant head reservoir into a deep annular groove in the upper endcap through four tangential inlet ports to provide circumferentially uniform flow. The fluid then passed through a flow-straightening section in the upper endcap consisting of two honeycomb sections (0.5 cm thick with a cell diameter of 0.1 cm) on either side of a 2:1 contraction section to straighten the flow and to provide an end boundary condition in the test section of nearly axial flow with minimal radial and azimuthal velocity components. The fluid exited the flow cell via a deep annular groove in the lower endcap. The axial volume flow rate was controlled by a valve downstream of the flow cell and measured with an electromagnetic flowmeter (Turbo Instruments, model MG711) at the exit of the flow cell. Fluid was recirculated to the upper constant-head reservoir by a pump. The deleterious effect of refraction at the curved inner and outer surfaces of the outer cylinder was eliminated by enclosing the outer cylinder in a square glass box and using a fluid having a refractive index matched to that of the glass both as the working fluid and to fill the space between the outer cylinder and the box.

The working fluid was a mixture of water, glycerol, sodium iodide to increase the solution's refractive index, and trace amounts of sodium thiosulfate to prevent a yellowish tint in the solution.[34] Silver-coated hollow glass spheres (Potters Industries, NJ) with an average diameter of 14 μm were added as seed particles in a volume concentration of 1.0×10^{-4}. The particles had a density of 1.6 g/cm^3, which was slightly less than the density of the working solution, 1.62 g/cm^3 as measured with a hydrometer. The particles reflect the light uniformly in all directions and were small enough to stay in suspension for several hours and accurately follow any velocity fluctuations in the flow.[35] The nominal kinematic viscosity of the solution was 3.15×10^{-6} m^2/s. The fluid temperature was measured before and after each experiment and varied by no more than 2 °C. The viscosity was measured at the beginning and end of each experiment using a Canon–Fenske viscometer.

In this paper the axial Reynolds number is defined as $\mathrm{Re} = wd/\nu$, where w is the average axial velocity based on the axial volume flow rate, d is the width of the annular gap, and ν is the kinematic viscosity. Although the Taylor number, which relates the centrifugal forces to the viscous forces, has several different forms, we use $Ta = r_i \Omega d / \nu$. where r_i is the radius of the inner cylinder and Ω is the rotational velocity of the inner cylinder. This form of the Taylor number, often called a rotating or inner Reynolds number, is used because it is simple and consistent with the form used in several recent studies.[9,28,29,36,37] In a typical series of experiments, the axial Reynolds number was set using a valve downstream of the flow cell. Then the speed of the inner cylinder was slowly, linearly ramped to obtain the desired Taylor number. The flow was allowed to reach steady state, usually about 15 min after reaching the desired rotation rate, before taking data. We estimate the uncertainty in the Reynolds number and Taylor number to be 3% to 4%, primarily due to variations in fluid viscosity and uncertainty in the dimensions of the apparatus.

The flow velocities were measured using a TSI, Inc. Particle Image Velocimetry (PIV) system based on cross-correlating a pair of images, thus eliminating directional ambiguity. An electronically shuttered 10 W argon laser was used to illuminate a meridional plane. The laser sheet had a thickness of 0.2 mm with $\pm 0.5\%$ variation in thickness in the measurement field and was carefully aligned in a meridional plane to avoid anomalous apparent radial velocity components caused by the azimuthal path of the particles through the thickness of the laser sheet. Since the through-sheet velocity in the azimuthal direction was so much larger than the measured axial and radial velocities, care was taken to assure that the laser sheet timing was short enough and the laser intensity great enough to capture a largely overlapping population of particles in two consecutive images, even near the

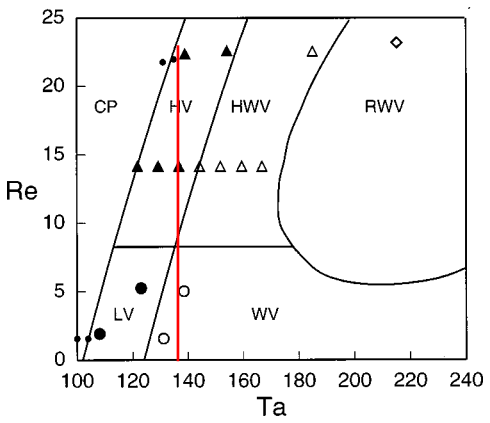

FIG. 2. Conditions at which experiments were conducted in the Ta-Re plane. Curves indicate approximate boundaries between flow regimes. Regimes include nonvortical Couette–Poiseuille (CP) flow (·), nonwavy laminar vortex (LV) flow (●), wavy vortex (WV) flow (○), nonwavy helical vortex (HV) flow (▲), helical wavy vortex (HWV) flow (△), and random wavy vortex (RWV) flow (◇).

inner cylinder where the through-sheet velocity is greatest. A TSI, Inc. Cross-Correlation CCD camera positioned perpendicular to the laser sheet was used to record the particle images in the illuminated plane about one-third of the flow cell height from the bottom of the flow cell, in the middle of the region where the flow is fully developed.

Images were acquired with a custom-written image acquisition program that allowed arbitrarily sized images to be collected at 30 Hz until the computer's memory was completely filled. Two different types of measurements were made in order to study both the spatial as well as the temporal dependence of the flow. For the spatial measurements, ~180 image pairs measuring 640 axially by 210 radially pixels were captured at a net rate of 15 Hz. The time between laser pulses for an image pair was 0.008–0.010 s. Velocity vectors were calculated at a grid of 31 points in the axial direction and 9 points in the radial direction using an interrogation region of 32 by 32 pixels. For frequency measurements, as many as 9000 small image pairs located at the center of the spatial measurement area and measuring 88 pixels axially and 32 pixels radially were sampled at 15 Hz.

The critical Taylor number at the onset of Taylor vortex flow for $\eta=0.83$ with no axial flow is $Ta_c=102$, based on a cubic spline fit to the data provided by DiPrima and Swinney.[38] The parameter space investigated in this paper is $100<Ta<215$ and $1.6<\mathrm{Re}_{ax}<23$. This parameter space includes several different flow regimes previously identified using flow visualization and spectral analysis of the light reflected from the seed particles in the flow field.[24,28,29] Figure 2 indicates the conditions in the Taylor number-Reynolds number plane at which measurements were made. The nature of the flow at those values was based on spectral analysis of the axial and radial velocity data sets using 9000 image pairs, similar to the methodology to detect the flow regime based on laser Doppler velocimetry and reflected light measurements.[39,40] The curves show the approximate boundaries between flow states, but these boundaries are not intended to represent the exact demarcation between flow regimes, since that was not the purpose of this study. The power spectrum of stable Couette–Poiseuille flow (CP) is featureless. The spectrum of nonwavy, nonhelical laminar vortices (LV) exhibits a single spectral peak related to the axial translation of vortices through the measurement region along with higher-order harmonics. Wavy vortex flow (WV) exhibits peaks related to the axial translation of vortices and the azimuthal waviness as well as linear combinations of these frequencies and their higher harmonics. Under certain conditions, the waviness takes on a random character (RWV) characterized by a broad fundamental peak. Toroidal and helical vortices cannot be easily differentiated using spectral analysis but are readily identified from flow visualization using a very low concentration of reflective titanium dioxide coated mica flakes[29] (5–25 μm across and about 0.5 μm thick, Superpearl 120c, Mearl Corp.).

III. VELOCITY VECTOR FIELDS

The raw velocity vector fields in the frame of reference of the apparatus are useful in obtaining a general sense of the flow field, but since the axial velocity related to the vortices is about the same magnitude or less than the axial velocity associated with the imposed axial flow the vortices are difficult to detect visually. One option is to view the vortices with the spatially averaged axial velocity subtracted from the velocity field,[41] which is equivalent to viewing the vortices in a reference frame translating at the average axial velocity of the flow. This permits the identification of individual vortices so that their motion can be followed, although the details of the vortex velocity field can be somewhat distorted, particularly near the walls of the annulus. Instead we subtracted the axially- and temporally-averaged axial velocity profile $\langle w\rangle$, which is a function of radius, from the velocity vector field. By removing the superposed axial velocity profile, the distortion of the vortex velocity field by the axial velocity profile is minimized making details of the vortices more clearly evident.

The normalized time- and space-averaged axial velocity profile that was subtracted from the instantaneous velocity field is shown in Fig. 3 for all five vortical flow states along with the theoretical axial velocity profile for stable, laminar annular Poiseuille flow. The averaged velocity profiles for unstable flow are remarkably similar to the stable theoretical velocity profile. The only difference seems to be the slightly fuller velocity profile near the inner cylinder resulting from a slight shift of the velocity profile toward the inner cylinder, apparently due to vortical transport of axial momentum toward the inner cylinder and consistent with previous hot-wire studies.[30,31] Also noteworthy is that the velocity profiles for the five different vortical flow states are quite similar to one another. Together these two results indicate that the vortical flow has only a very small effect on the axial velocity profile and that the effect is largely independent of the details of the vortical flow state.

A. Nonwavy vortices

An example of the time series of the velocity field for nonwavy, nonhelical laminar vortices (LV) with the axial

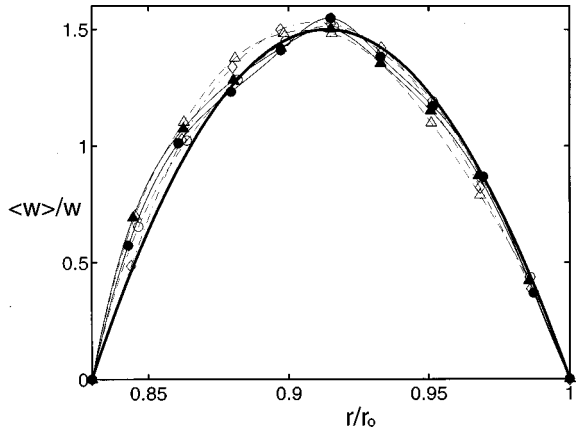

FIG. 3. The normalized average axial velocity profile for nonwavy laminar vortex ($Ta=123$, Re=5.3) flow (●, solid curve), wavy vortex ($Ta=139$, Re=5.0) flow (○, dashed curve), nonwavy helical vortex ($Ta=129$, Re =14.2) flow (▲, solid curve), helical wavy vortex ($Ta=167$, Re=14.2) flow (△, dashed curve) and random wavy vortex ($Ta=215$, Re=23.2) flow (◇, dot–dash curve). All curves are interpolated through the data using cubic splines. The theoretical velocity profile for stable, laminar annular Poiseuille flow is shown as a heavy solid curve.

velocity profile removed is shown in Fig. 4. In this and subsequent figures, the velocity field is shown at several time instants with time progressing from top to bottom. Since the velocity field repeats over a readily measured time period, the velocity field was ensemble-averaged over several realizations. The upper line at each time instant represents the rotating inner cylinder, and the lower line represents the stationary outer cylinder. Vortex centers are marked with an asterisk based on the interpolated position of minimum speed in the meridional plane, $(v_r^2+v_z^2)^{1/2}$, using a weighted average over a 3×3 neighborhood of spatially adjacent measurement points. The left to right axial flow is evident from the rightward translation of the vortex centers. At any given time

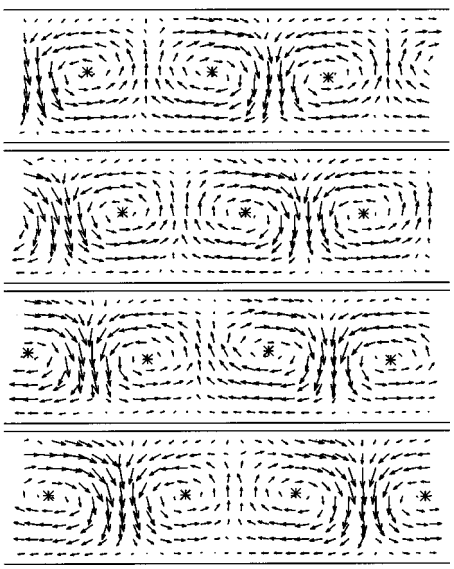

FIG. 4. Time series for nonwavy laminar vortex flow at $Ta=123$ and Re =5.3 with the axial velocity profile removed. Time progresses from top to bottom. The upper line in each frame is the rotating inner cylinder: the lower line is the stationary outer cylinder. Time between frames is 1.025 s.

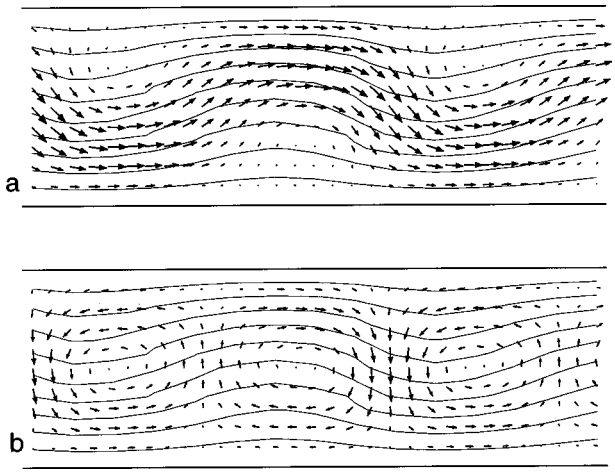

FIG. 5. Radial and axial velocity vectors with azimuthal velocity contours at $Ta=123$ and Re=5.3. The upper line in each frame is the rotating inner cylinder; the lower line is the stationary outer cylinder. The contours represent the azimuthal velocity normalized by the speed of the inner cylinder, thus ranging from 1.0 at the inner cylinder to 0.0 at the outer cylinder in steps of 0.1. The length of the velocity vectors (L_v) divided by the gap width (d) in the figure represents the velocity normalized by the speed of the inner cylinder. (a) Velocity field including the axial velocity profile. (b) Velocity field with the axial velocity profile removed.

instant, the flow looks almost identical to nonwavy vortex flow with no axial flow.[42] For instance, the vortex cells are nearly square, the outflow is substantially stronger than the inflow, and there is negligible cross flow between vortices. Nevertheless, the left-to-right axial translation of vortices as shape-constant units from frame to frame resulting from the axial flow is clearly evident.

Figure 5 shows the azimuthal velocity contours superposed on the velocity vector field for the nonwavy, nonhelical vortices shown in Fig. 4. The length of the velocity vectors (L_v) divided by the gap width (d) in the figure represents the velocity normalized by the speed of the inner cylinder ($v/\Omega r_i=L_v/d$). Figure 5(a) shows the axial-radial velocity vectors as measured in the frame of reference attached to the apparatus. The left-to-right axial flow is evident as a strong stream of fluid winding around vortices that do not fill the annular gap and appear alternately displaced toward the inner and outer cylinders. In our previous papers we have called this ''winding'' flow.[33,41] Removing the axial velocity profile, shown in Fig. 5(b), results in vortices that fill the gap, are centered in it, and have stronger outflow regions than inflow regions. In fact, these vortices appear nearly the same as they would with no axial flow imposed. As shown in Fig. 3, the spatially averaged axial velocity profile that has been removed in going from Fig. 5(a) to Figure 5(b) is nearly identical to the velocity profile for stable laminar Poiseuille flow in an annulus. Thus, it appears that winding flow is nearly a linear superposition of annular Poiseuille flow and nonwavy Taylor vortex flow.

The azimuthal velocity component for nonwavy flow can be calculated numerically from the radial and axial velocity components using the azimuthal momentum equation and noting the axisymmetry of the flow.[42] The calculation is performed by resampling the experimental measurements

onto a uniform grid, finite differencing the azimuthal momentum equation, and solving the resulting system of linear simultaneous equations using matrix methods. The no-slip boundary condition is imposed at the inner and outer cylinders. To minimize numerical errors related to random error in the velocity field data, this procedure works best on ensemble averaged velocity fields. Since the shapes of the vortices do not change, the velocity fields can be averaged over the entire data set by shifting each data set axially by an amount equal to the axial propagation distance of the vortices relative to the first set to generate an ensemble averaged velocity field. The resulting azimuthal velocity contours in Fig. 5 are distorted from the straight horizontal contours that would appear if no vortices were present. The cause of the distortion of the azimuthal velocity contours is clear from the lower part of the figure, where the axially averaged mean axial velocity profile has been subtracted from the vectors. The vortices advect high azimuthal momentum fluid from near the inner cylinder outward and low azimuthal momentum fluid from near the outer cylinder inward. When an axial flow is present, the extrema are somewhat downstream of the inflow or outflow regions. This result is different from that for nonwavy Taylor vortex flow with no axial flow[42] where the extrema in the bulges of the contours are exactly aligned with the inflow or outflow regions between vortices. The imposed axial flow transports azimuthal momentum downstream at the same time that it is being carried radially, shifting the extrema in the azimuthal velocity contours downstream from the radial outflow regions. Measurements at other axial Reynolds numbers clearly show that the offset of the extrema from the inflow–outflow regions increases with the axial flow rate confirming that the shift in the extrema is a result of the axial transport of azimuthal momentum.

At higher axial Reynolds numbers for which the vortices become helical, the character of the flow field changes significantly as shown in Fig. 6(a), where the velocity normalized by the speed of the inner cylinder is equal to a scaling factor A times the length of the velocity vectors divided by the gap width ($v/\Omega r_i = AL_v/d$). The stronger axial flow related to the higher axial Reynolds number necessary to achieve helical vortices is evident in the seeming disappearance of the vortices altogether for the velocity field as measured. Here the imposed axial flow is so strong that it overwhelms the velocity related to the vortical motion. The only evidence of the vortices is the sinuous nature of the axial flow. However, when the axially averaged mean axial velocity profile is subtracted from the data, the vortices are readily apparent, as shown in Fig. 6(b). The vortices appear similar to those in Fig. 5(b), in spite of their being helical rather than toroidal. The azimuthal velocity component was calculated for nonwavy helical vortices (HV) in the same manner as was done for the nonhelical vortices. In this case the axisymmetry is broken by the helical inclination of the vortices, but since the helical inclination is slight, less than 5°,[29,32] the resulting error is minimal if axisymmetry is assumed. Again the azimuthal velocity contours are distorted by the axial flow, but not nearly so much as at the lower axial Reynolds number in Fig. 5 in spite of the similar Taylor numbers. This effect can be attributed to the higher axial velocity. The axial location of the extrema in this case are shifted more than in Fig. 5, so that they are nearly aligned with the vortex centers rather than the inflow–outflow regions demonstrating the strong effect of the axial flow on the radial transport of azimuthal momentum.

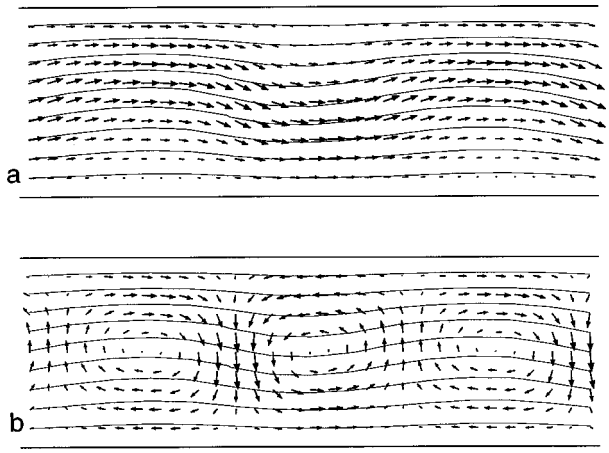

FIG. 6. Radial and axial velocity vectors for helical vortex (HV) flow at $Ta = 129$ and $\mathrm{Re} = 14.2$. The contours represent the azimuthal velocity normalized by the speed of the inner cylinder, thus ranging from 1.0 at the inner cylinder to 0.0 at the outer cylinder in steps of 0.1. (a) Velocity field including the axial velocity profile. (b) Velocity field with the axial velocity profile removed. The length of the velocity vectors divided by the gap width in the figure represent $A = 0.5$ times the velocity normalized by the speed of the inner cylinder for (a) and $A = 1.25$ times the velocity normalized by the speed of the inner cylinder for (b).

The measurements shown in Figs. 5 and 6 and similar measurements for the LV and HV flow regimes have some general trends. First, the inflow and outflow regions consist almost entirely of radial velocity once the axial velocity profile has been removed, indicating that there is very little axial transport between vortices due to the vortical motion itself. Nearly all of the axial fluid transport between vortices is a result of the imposed axial flow. Second, the vortical flow advects high azimuthal momentum outward from the inner cylinder and low azimuthal momentum inward from the outer cylinder. This effect increases with increasing Taylor number as the vortices get stronger. Third, the axial flow advects the azimuthal momentum, axially shifting the minimum and maximum displacement of the azimuthal velocity contours downstream. Finally, when the axial velocity profile is removed, the vortices remain centered in the annulus regardless of the axial Reynolds number. Thus, the appearance of a winding flow in a frame of reference attached to the apparatus [Fig. 6(a)] is simply due to the superposition of the annular axial flow and the vortical flow. The ratio Ta/Re, which represents the relative strength of centrifugal effects to axial momentum effects, is useful to characterize the nature of the flow field in the reference frame attached to the apparatus.[31,33] For Fig. 5(a), $Ta/\mathrm{Re} \approx 23$ is large indicating relatively strong vortices that, though displaced toward the walls of the annulus, are readily evident in the figure. However in Fig. 6(a), $Ta/\mathrm{Re} \approx 9$ is smaller indicating stronger axial flow resulting in a winding flow without visible vortices.

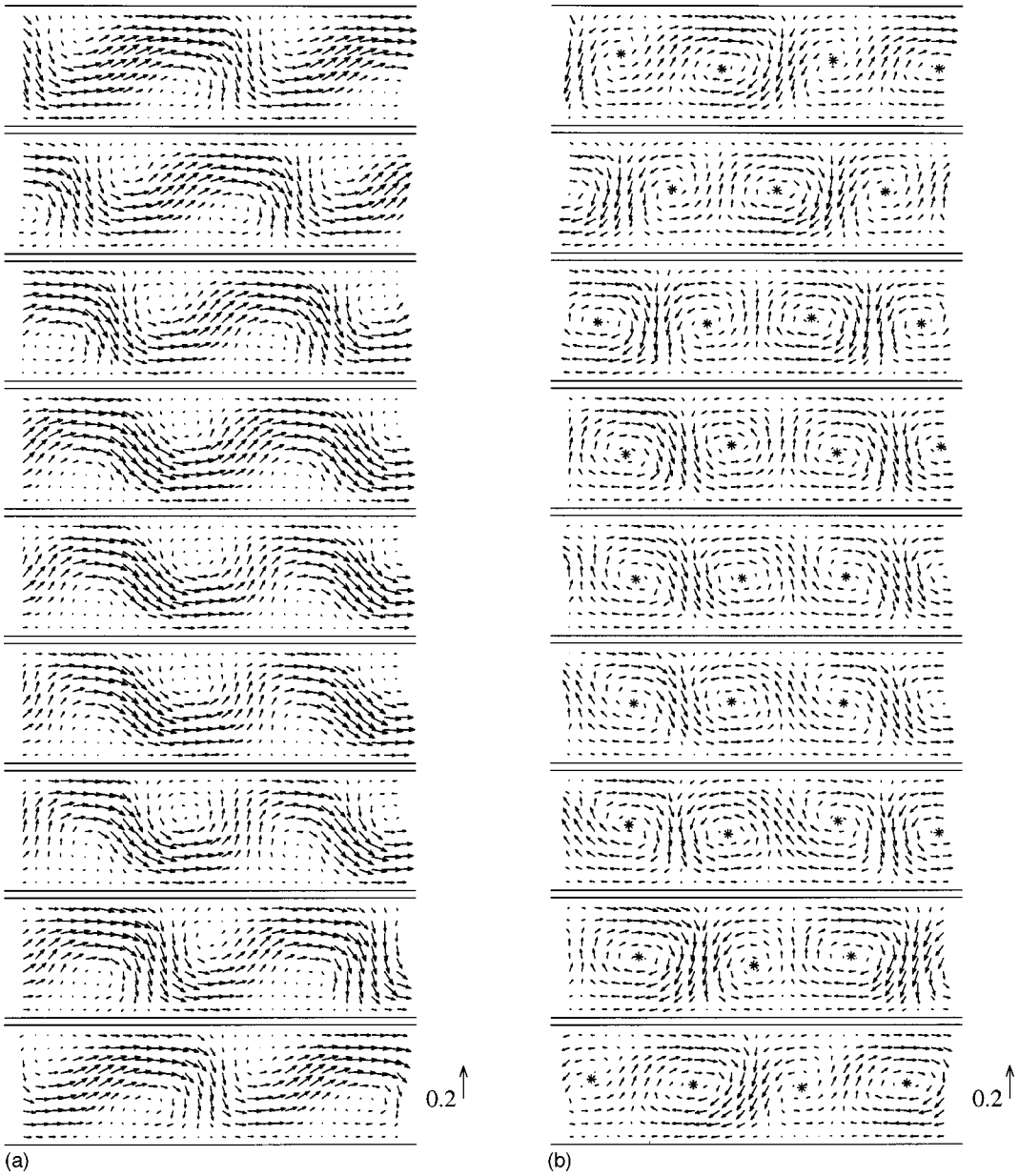

FIG. 7. Radial and axial velocity vectors for wavy vortex (WV) flow at $Ta=139$ and $\mathrm{Re}=5.0$. Frames are shown for 9 time steps (from top to bottom) spanning the period of one traveling wave, with the first and last frames representing the same phase in the traveling wave. (a) Velocity field including the axial velocity profile. (b) Velocity field with the axial velocity profile removed. The arrow in the lower right corner represents $0.2\Omega r_i$.

B. Wavy vortices

At higher Taylor numbers the vortices acquire an azimuthal waviness. In this case, ensemble averaging the velocity fields without removing the features of interest is quite difficult since two phenomena, axial translation and azimuthal traveling waves, occur at incommensurate frequencies. As a result, there is no time period over which the velocity field will repeat exactly. So averaging was carried out by ensemble averaging consecutive image pairs over a time period of 4% of the azimuthal wave period, which ranged from one image pair to four image pairs. We consider three cases of wavy vortex flow: Wavy toroidal vortices, wavy helical vortices, and random wavy vortices.

The velocity field for nonhelical wavy vortex (WV) flow is shown in Fig. 7. Here and in subsequent figures, the velocity field at nine time instants is shown with time progressing from top to bottom. Eight time instants correspond to the period of one azimuthal wave of the wavy vortex, so that the first and ninth frames depict the same phase of the azimuthal wave. Comparison of the first and last (ninth) frames illustrates the axial translation of the vortices over the period of one azimuthal wave. Before the axial velocity profile is subtracted from the vectors, the winding axial flow is clearly evident in Fig. 7(a). The nonuniform translation velocity of the vortices is evident after the axial velocity profile is removed, as shown in Fig. 7(b). For instance, the counterclockwise vortex on the left side of the first frame moves downstream (right) in frames 1–4, but then moves upstream in frames 5 and 6, before continuing downstream in frames 7–9. The retrograde motion is related to the azimuthal wavi-

ness. In the case of no axial flow, the traveling wave passing through a particular meridional plane results in the appearance of the vortex center oscillating axially.[42] In Fig. 7(b), the axial oscillations related to the azimuthal traveling wave add to the axial translation of the vortex due to the axial flow. When the portion of the vortex in the meridional measurement plane is moving axially against the axial flow, the vortex center moves retrograde to the axial flow. Thus, the vortices in Fig. 7(b) oscillate axially due to the passage of the azimuthal waviness of the wavy vortex, while continually making progress in the same direction as the net axial flow.

A fundamental difference between wavy vortex flow and toroidal vortex flow, each with no imposed axial flow, is that a significant portion of fluid is transferred from one vortex to another for wavy vortices,[42,43] whereas toroidal vortices are essentially closed cells. When the axial velocity profile is subtracted from the vector field the cyclic transfer of fluid between vortices inherent in wavy vortex flow without an imposed axial flow[42] is apparent, as shown in Fig. 7(b). The cycle of transport between vortices is evident when one considers a particular vortex, say the leftmost vortex in the first frame. At certain times during the cycle (frames 4–7) the vortex grows as it fills with fluid from neighboring vortices, while at other times (frames 1, 2, 8, and 9) it shrinks as it loses fluid to its adjacent vortices. Similar growth and shrinkage of wavy vortices occurs when there is no axial flow.[42] However, at certain instants during the cycle of one wave passing the measurement plane in the case of no imposed axial flow, there is an instantaneous net axial flow as fluid winds around vortices. This type of instantaneous axial flow related to the waviness is not apparent in Fig. 7(b), although it does appear at higher Taylor numbers even with an imposed axial flow.

At higher axial Reynolds numbers the vortices are helical wavy vortices (HWV). Figure 8 shows wavy helical vortices at $\mathrm{Re}=14.2$ and $Ta=167$, somewhat above the transition to waviness. The flow winding around the vortices is quite evident before the axial velocity profile is removed from the data, shown in Fig. 8(a). When the axial velocity profile is removed from the data, shown in Fig. 8(b), the flow closely resembles that of wavy vortex flow without an imposed axial flow in that there is significant transfer of fluid between adjacent vortices at certain points in the cycle. In addition, there are instances where there is a net axial flow winding around the vortices even after the axial velocity profile has been removed, similar to the case with no axial flow.[42] For instance, in frame 3 fluid winds around the vortices to the left, opposite to the net axial flow.

The helical nature of the flow is not evident from the meridional plane velocity field shown in Fig. 8(b), and the waviness of the flow is somewhat difficult to detect from the velocity field. However, close examination of the leftmost vortex in frame 1 indicates that the vortex moves to the right more slowly in frames 1–3 than in frames 4–6, slowing down again in frame 7 before it exits the measurement domain. Furthermore, the power spectrum of the velocity field clearly shows an additional peak characteristic of the waviness.

At higher Taylor numbers and axial Reynolds numbers the flow gives way to random wavy vortex (RWV) flow. This flow is characterized by wavy vortices that change shape rapidly, may be helical or toroidal, and often display dislocations where a two vortex pairs on one side of the cylinder appear to merge into a single vortex pair on the opposite side of the cylinder.[29] The velocity vector fields shown in Fig. 9 depict the random nature of the flow. At some time instants, for example frames 4–6, the flow is similar to that for helical flow in Fig. 8. Before subtracting the axial velocity profile, the fluid appears to wind around vortices, shown in Fig. 9(a). After subtracting the axial velocity profile, shown in Fig. 9(b), the transfer of fluid between vortices characteristic of wavy vortex flow are evident in frames 4–6, although the flow is less well ordered than in Fig. 8(b). But at other times, the character of the flow is much different. The vortices are not evident at all for some time instants before the axial velocity profile is removed from the data [frames 2 and 3 in Fig. 9(a)]. The velocity fields with the axial velocity profile removed. Fig. 9(b), demonstrate the randomness in the flow even more clearly. The vortices often change substantially in shape, size, and separation as they translate axially. In some frames (1, 2, 4, and 9), a net axial flow apart from the imposed axial flow is evident. At times the vortices appear strong and fill the annulus (frames 5 and 7), while at other times the vortices are quite weak (frames 2 and 3), displaced against one wall (frame 4), or displaced against opposite walls (frames 1 and 6).

We have observed dislocations where one vortex catches up with the next downstream vortex so that they are side by side at the same axial location but are substantially weaker than the surrounding vortices upstream or downstream of them. The side-by-side vortices obliterate each other and disappear as a pair to maintain the counter-rotation of the remaining vortices. It is likely that this dislocation mechanism is related to the interaction between the axial transfer of fluid characteristic of wavy vortices and the imposed axial-through flow.

It is difficult to observe any oscillations in the axial position that could be related to the axial motion of the vortex center due to the waviness of the vortex in Fig. 9, though flow visualization using reflective flakes and frequency measurements based on PIV data clearly show the presence of wavy vortices with a random character. Apparently the axial motion due to the waviness is so much smaller than the axial motion of the vortices due to the imposed axial flow and is so random in its occurrence that it is not detectable within the resolution of our measurements.

IV. FLOW STATE PROPERTIES

Based on the velocity vector fields, various spatio-temporal properties of the Taylor–Couette flow with an imposed axial flow can be examined. We first address the wavelength of the vortices and their axial motion. The axial velocity of a vortex, w_{vortex}, is related to the wavelength of a vortex pair, λ, and frequency of vortices passing a point due to the axial motion, f_{ax}, through $w_{\mathrm{vortex}}=\lambda f_{\mathrm{ax}}$.

Consider first the frequency due to the axial translation of vortices, f_{ax}, calculated from the power spectrum of the

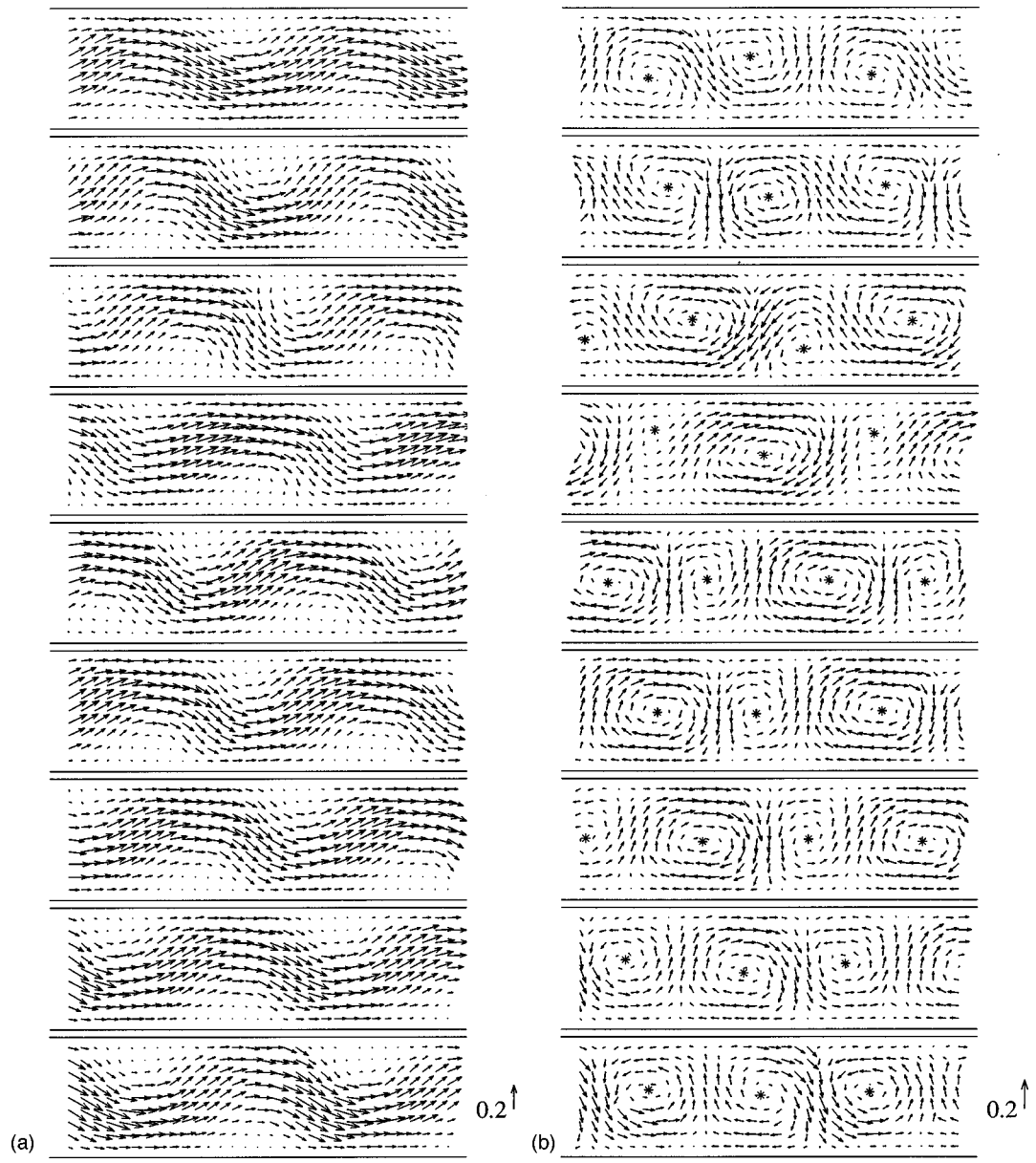

FIG. 8. Radial and axial velocity vectors for helical wavy vortex (HWV) flow at $Ta=167$ and $\mathrm{Re}=14.2$. Frames are shown for 9 time steps (from top to bottom) spanning the period of one traveling wave, with the first and last frames representing the same phase in the traveling wave. (a) Velocity field including the axial velocity profile. (b) Velocity field with the axial velocity profile removed. The arrow in the lower right corner represents $0.2\Omega r_i$.

velocity fields. For nonhelical, nonwavy vortical flow (LV), linear stability theory and experiments indicate that f_{ax} is proportional to the average axial velocity of the flow and thereby coupled directly to the axial Reynolds number at transition to vortical flow.[8,11] But there is a slight dependence of f_{ax} on Ta for the two LV data points in Fig. 10. For these two points Re differs by a factor of 2.8, but f_{ax} differs by a factor of 2.5. This suggests a slight dependence of the axial motion of the vortices upon Ta in addition to dependence on Re, once Ta is above that for transition to vortical flow.

For helical states (HV, HWV, RWV), the frequency of vortex passage, f_{ax}, is directly related to the rotational frequency of the inner cylinder, f_{ic}, as shown by the linear relation in Fig. 10. The least-squares line fit to the helical states is $f_{\mathrm{ax}}=2.01f_{\mathrm{ic}}$ with an R^2 value of 0.9998. The data points on this line include all eleven nonwavy helical, wavy helical, and random wavy vortex states (two pairs of points overlay each other) for $\mathrm{Re}_{\mathrm{ax}}=14.2$ or 22.4 and $122\leqslant Ta\leqslant 215$. Thus, it appears that the axial translation of the helical vortices is directly coupled to the Taylor number, independent of the axial Reynolds number. (We intentionally plotted f_{ax} as a function of f_{ic} rather than as a function of Ta to most clearly show the relation. If Ta is used, slight differences in viscosity from experiment to experiment result in slightly more deviation from the linear fit through the data.) We are aware of no theoretical basis for this relationship, although some evidence of a linear relationship between the frequency for the axial translation of vortices and the frequency of the inner cylinder can be extracted from the results for stability analysis for helical vortices.[9] There are too few data points for nonhelical wavy vortices (WV) to determine

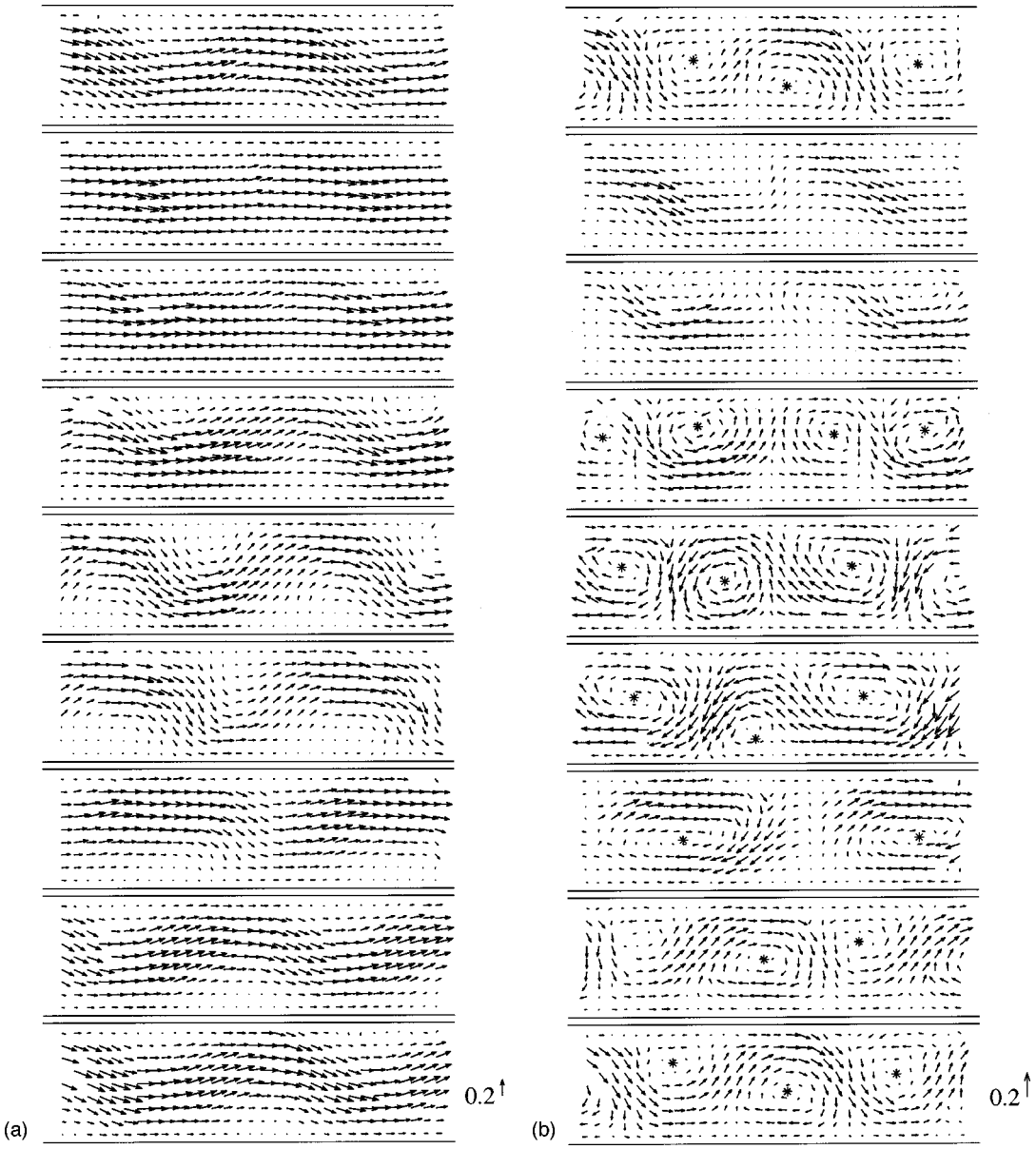

FIG. 9. Radial and axial velocity vectors for random wavy vortex (RWV) flow at $Ta=215$ and Re=23.2. Frames are shown for 9 time steps (from top to bottom) spanning the period of one traveling wave, with the first and last frames representing the same phase in the traveling wave. (a) Velocity field including the axial velocity profile. (b) Velocity field with the axial velocity profile removed. The arrow in the lower right corner represents $0.2\Omega r_i$.

the dependence of the vortex passage frequency on inner cylinder rotation.

Figure 11 shows the wavelength λ of a pair of vortices normalized by the gap width. The vortex pair wavelengths were calculated by finding a maximum in the autocorrelation of the radial and axial velocity components and are, therefore, based on the velocity field across the entire gap width. The results are consistent with the approximate flow visualization measurements at similar Reynolds and Taylor numbers.[29] Clearly there is substantial variation in the vortex pair height. At transition from stable flow to nonhelical Taylor vortex flow the theoretical pair height is almost exactly $2d$ for $\eta=0.83$.[8] In nearly all cases, regardless of the structure of the vortices, the wavelength is less than this value for Taylor numbers above the critical Taylor number. This trend is particularly evident for a particular series of data, helical vortices for $\mathrm{Re}_{ax}=14$ and $122\leqslant Ta\leqslant 152$ (large triangles). For the five data points at low Ta there is a linear dependence of the pair height on the Taylor number as shown by the linear regression fit in Fig. 11 for helical and weakly wavy helical vortices. The linear trend is broken between $Ta=152$ and $Ta=160$ where the pair height suddenly increases by 20%. There are too few data points at other axial Reynolds numbers to determine if similar trends occur.

The vortex translation speed normalized with the average axial velocity shown in Fig. 12 was determined from the vortex pair wavelength and the frequency of axial passage of vortices, $w_{\mathrm{vortex}}=\lambda f_{ax}$. We also include data obtained in an early similar study in our lab based on the translation speed of the vortex centers for $3\leqslant \mathrm{Re}_{ax}\leqslant 33$ and $110\leqslant Ta\leqslant 320$.[41] Clearly, the normalized velocity of the vortices is indepen-

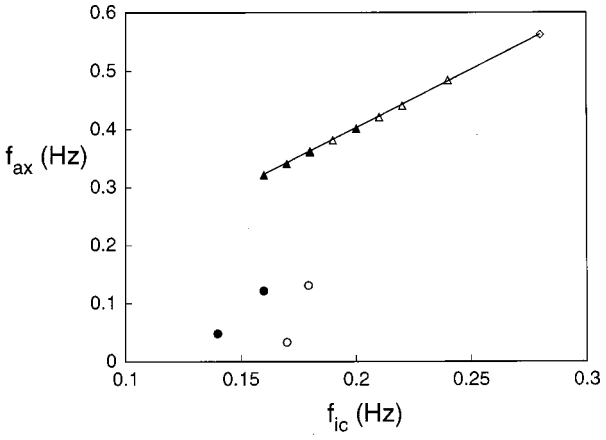

FIG. 10. Frequency of vortex passage, f_{ax}, as a function of inner cylinder frequency $f_{ic}=\Omega/2\pi$, for nonwavy laminar vortex (LV) flow (●), wavy vortex (WV) flow (○), nonwavy helical vortex (HV) flow (▲), helical wavy vortex (HWV) flow (△), and random wavy vortex (RWV) flow (◇). The trend line for helical and random wavy states is for conditions of $\mathrm{Re}_{ax}=14.2$ or 22.4 and $122\leqslant Ta\leqslant 215$.

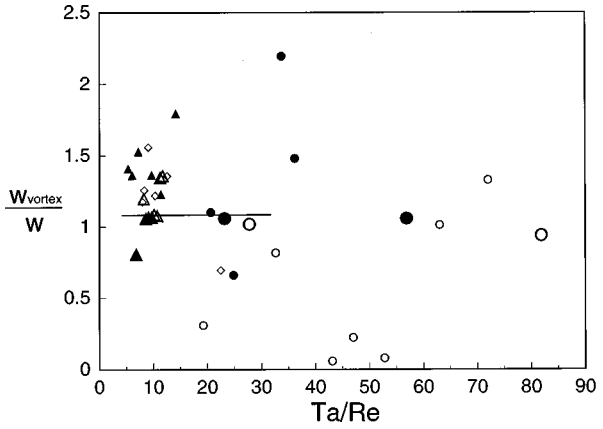

FIG. 12. Vortex translation speed normalized by the mean axial velocity as a function of Ta/Re for nonwavy laminar vortex (LV) flow (●), wavy vortex (WV) flow (○), nonwavy helical vortex (HV) flow (▲), helical wavy vortex (HWV) flow (△), and random wavy vortex (RWV) flow (◇). Large symbols are results from frequency of vortex passage (current study); small symbols are from measurements of vortex speed (Ref. 41).

dent of the flow regime, the axial velocity of the fluid, and the parameters of the flow. Plotting the same data against Re or Ta rather than Ta/Re, results in a similar random distribution of data.

The theoretical vortex translation speed for nonwavy toroidal vortices is also shown on Fig. 12.[8] The theoretical value of $w_{\mathrm{vortex}}/w=1.17$ is based on linear interpolation of the theoretical results for a radius ratio of $\eta=0.83$ at axial Reynolds numbers from 1.6 (the minimum Reynolds number that we considered) to 20 (the maximum Reynolds number for which the analysis is valid). The experimentally measured vortex translation speeds for toroidal vortices are near the theory in some cases. The deviation of the experiment from the theory in other cases is most likely a consequence of the theory being applicable only at transition from stable to supercritical flow, whereas the experimental data is well above the critical Taylor number. At the lowest ratios of Ta/Re ($Ta/\mathrm{Re}<12$), the normalized vortex velocity remains within a smaller band than at higher ratios of Ta/Re. Perhaps the relatively strong axial flow carries the vortices along with it largely unaffected by the character of the vortices for low ratios of Ta/Re. At larger ratios of Ta/Re, the vortical flow is prominent so that it may exert a stronger influence on the axial translation of vortices. An example is the nearly stationary wavy vortices ($w_{\mathrm{vortex}}\approx 0$) at $43\leqslant Ta/\mathrm{Re}\leqslant 53$. An island of nearly stationary vortices within the region of translating vortex flow has been noted by other researchers,[28,29] but the vortices were helical, not wavy. Stationary nonhelical, nonwavy vortices have also been observed in two-liquid flows,[44] and under the condition of very low Reynolds number.[13] In any case, no explanation has yet been offered regarding the physics behind the appearance of nearly stationary vortices in certain small regions of the Re-*Ta* parameter space. The vortices in this case appear nearly as they would with no axial flow at all. The vortex centers follow nearly closed elliptical paths along the centerline of the annulus, which is typical of wavy vortex flow with no axial flow.[42]

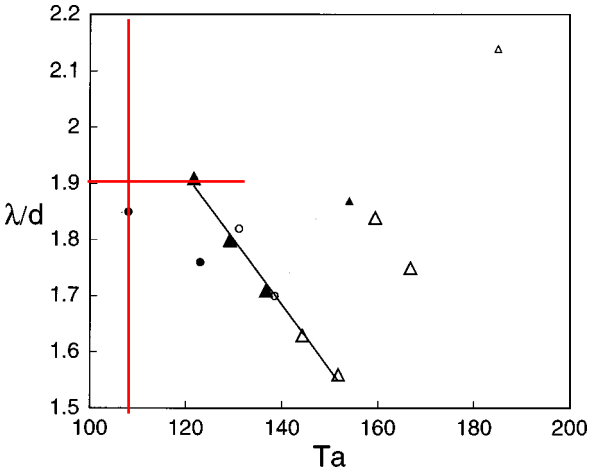

FIG. 11. Vortex pair wavelength as a function of Taylor number for nonwavy laminar vortex (LV) flow (●), wavy vortex (WV) flow (○), non-wavy helical vortex (HV) flow (▲), and helical wavy vortex (HWV) flow (△). The wavelength for random wavy vortex flow could not be measured due to the randomness of the flow. Large symbols are data points for Re=14. The line indicates a trend in the Re=14 data at low Ta.

The absence of any trend in the data in Fig. 12 (or when the same data is plotted versus Re or Ta) suggests that there is no general relationship between the vortex translation speed and the axial velocity of the fluid, even though at transition to vortical flow an exact relation exists. The strong dependence of supercritical cylindrical Couette flows on startup conditions[45] and details of the apparatus, suggests that the vortex translation speed, like the general character of supercritical wavy vortex flow, is strongly dependent on geometric details of the apparatus and/or the procedure to reach the final operating conditions.

Recent measurements of the velocity field in wavy Taylor vortex flow with no axial flow have shown that significant fluid volume is transferred axially across vortex boundaries due to fluid winding around the vortices.[42] The direction of the axial transfer of fluid due to the waviness is

the same as the direction of the axial displacement of the vortices due to the waviness. The instantaneous axial Reynolds number related to the axial flow between vortices with no imposed axial flow can be as large as the axial Reynolds number due to the imposed axial flow in this paper. Thus, a key question is the relative importance of the instantaneous axial transfer of fluid between vortices that is due to the waviness of the vortices compared to the imposed axial flow.

To address this issue, the volume flow rate across a vortex boundary was determined as a fraction of the volume flow rate due to the imposed axial flow by finding the net fluid volume transferred across a vortex boundary after the axially averaged axial velocity profile was removed from the velocity field. We calculate the net volume of fluid flowing across a vortex boundary, Q_{net}, for a situation like that shown in Fig. 8(b) over several azimuthal waves. This is done by first finding the vortex boundary, defined as the instantaneous axial location at which extrema in the radially averaged radial velocity occur (corresponding to radial inflow and outflow regions). This is followed by numerically integrating the axial flow across that axial position to get Q_{net} at that instant. The time-averaged volume of fluid transferred, $\langle Q_{\mathrm{net}} \rangle$, represents the net average axial flow rate across vortex boundaries. The net volume transferred between vortices is expressed as the net flow rate across vortex boundaries normalized by the flow rate of the imposed axial flow, or

$$\frac{\langle Q_{\mathrm{net}} \rangle}{w \pi (r_o^2 - r_i^2)}.$$

The net volume transferred represents fluid flowing across the vortex boundaries due to the difference between the instantaneous axial velocity profile at the vortex boundaries and the time averaged axial velocity profile. In addition to the net fluid volume transferred across vortex boundaries, the total volume transferred across the vortex boundaries can be calculated based on the absolute value of the difference between the instantaneous velocity profile at the vortex boundary and the time averaged axial velocity profile. Since the total volume transferred between vortices includes flow into and out of a vortex at the vortex boundary, it represents the degree of mixing of fluid between vortices.

The net fractional volume transferred between vortices is shown in Fig. 13(a). Negative net volume transferred indicates that fluid is transferred upstream, and vice versa. In nearly all cases, the net volume transferred is less than $\pm 6\%$ of the imposed axial flow rate. This small net volume transfer indicates that the flow is indeed very nearly a superposition of the vortex motion and the axially averaged axial velocity profile. This is a somewhat surprising result in that one might expect the no-slip condition on the axial velocity profile to cause some sort of distortion of the vortices that could lead to transfer of fluid across vortex boundaries, especially given that the vortex translation velocity can be quite different from the average axial velocity of the fluid.

The total fractional volume transferred across vortex boundaries is indicated in Fig. 13(b). For nonwavy vortices (filled symbols), the total volume transferred is relatively small indicating nearly independent vortex cells. Again this result is surprising given the axial velocity profile, and it suggests that the vortices are quite robust in spite of the imposed axial velocity. Nevertheless, this result is consistent with the appearance of the velocity field after subtracting off the mean axial velocity profile. For wavy vortices (open symbols), the fractional volume transferred is significant, which is consistent with the high degree of fluid transport between vortices characteristic of wavy vortices with no imposed axial flow.[42]

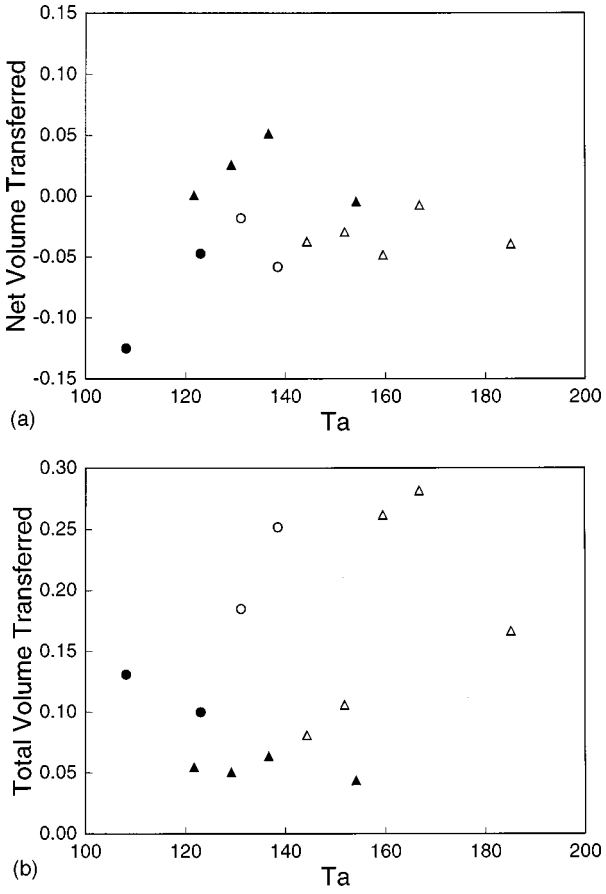

FIG. 13. Volume flow rate across vortex boundaries as a fraction of the axial volume flow rate for nonwavy laminar vortex (LV) flow (●), wavy vortex (WV) flow (○), nonwavy helical vortex (HV) flow (▲), and helical wavy vortex (HWV) flow (△). (a) Net volume transferred. (b) Total volume transferred.

V. SUMMARY

Previous research has shown a rich variety of flow regimes that can occur for cylindrical Couette flow with an imposed axial flow, depending upon Taylor number and Reynolds numbers. It would seem likely that the interplay between the imposed axial flow and the Taylor vortices would result in significant distortion of the vortices. The velocity fields for nonwavy vortices show the axial flow winding around vortices or even overwhelming the vortices so that the vortices are not even apparent. But when the axial velocity profile is removed, the velocity field in a meridional plane looks much like it would with no imposed axial flow except that the vortices translate axially and the distortion of

the azimuthal velocity contours due to the vortices is shifted axially by the axial flow. Consequently, the flow is essentially the linear superposition of the Taylor vortex flow and the imposed axial flow. The idea of superposition is supported when the transport of fluid between vortices is considered. For nonwavy vortices, there is little vortex-to-vortex transport of fluid in spite of the axial flow, consistent with the idea of independent vortex cells.

The velocity vector fields for wavy vortices also show axial flow winding around the vortices. Again, removing the axial velocity profile results in a flow that appears similar to that with no axial flow. For wavy vortices the inter-vortex fluid transport is substantial, much like the case of wavy vortices with no axial flow. For wavy vortex flow at low Reynolds numbers, the vortices generally translate along with the axial flow, but may move retrograde to the axial flow when the axial motion due to the waviness is opposite that of the axial flow. At higher Taylor and Reynolds numbers vortices are wavy and more random in their character. The effect of waviness on the motion of the vortices is not as clearly evident, because the velocity due to the waviness is small compared to the axial flow. Random wavy vortices translate generally axially, but with random deviations from this path. Sometimes the vortices are not easily observable. In addition, random wavy vortices disappear via a mechanism where two vortices move side by side, interact, and then disintegrate. In certain circumstances stationary wavy vortices appear with paths that are nearly closed loops, much like those for wavy vortices with no axial flow.

The velocity of the vortices in many cases is near the theoretical value at the transition to supercritical flow of 1.17 times the average axial velocity. But the range of vortex velocities is quite wide, especially when the vortices are strong compared to the axial flow (large Ta/Re), perhaps related to the sensitivity of vortex structure to details of the way the flow is initiated or the flow cell geometry. Likewise, the range of wavelengths of vortices is broad. For helical vortices the frequency of passage of the vortices past a point is directly related to the frequency of the inner cylinder rotation, although there appears to be no theoretical basis for this relationship.

ACKNOWLEDGMENTS

The support of the National Science Foundation is gratefully acknowledged. Malte Stöckert performed significant preliminary experiments[41] leading to those described here and was supported by the Deutsch Agentur für Raumfahrt Angelegenheiten (DARA).

[1] G. I. Taylor, ''Stability of a viscous liquid contained between two rotating cylinders,'' Philos. Trans. R. Soc. London, Ser. A **223**, 289 (1923).
[2] S. Chandrasekhar, ''The hydrodynamic stability of viscid flow between coaxial cylinders,'' Proc. Natl. Acad. Sci. USA **46**, 141 (1960).
[3] R. C. DiPrima, ''The stability of a viscous fluid between rotating cylinders with an axial flow,'' J. Fluid Mech. **9**, 621 (1960).
[4] S. Chandrasekhar, ''The stability of spiral flow between rotating cylinders,'' Proc. R. Soc. London, Ser. A **265**, 188 (1962).
[5] M. A. Hasoon and B. W. Martin, ''The stability of viscous axial flow in an annulus with a rotating inner cylinder,'' Proc. R. Soc. London, Ser. A **352**, 351 (1977).
[6] R. C. DiPrima and A. Pridor, ''The stability of viscous flow between rotating concentric cylinders with an axial flow,'' Proc. R. Soc. London, Ser. A **366**, 555 (1979).
[7] B. S. Ng and E. R. Turner, ''On the linear stability of spiral flow between rotating cylinders,'' Proc. R. Soc. London, Ser. A **382**, 83 (1982).
[8] A. Recktenwald, M. Lücke, and H. W. Müller, ''Taylor vortex formation in axial through-flow: Linear and weakly nonlinear analysis,'' Phys. Rev. E **48**, 4444 (1993).
[9] K. C. Chung and K. N. Astill, ''Hydrodynamic instability of viscous flow between rotating coaxial cylinders with fully developed axial flow,'' J. Fluid Mech. **81**, 641 (1977).
[10] D. I. Takeuchi and D. F. Jankowski, ''A numerical and experimental investigation of the stability of spiral Poiseuille flow,'' J. Fluid Mech. **102**, 101 (1981).
[11] H. A. Snyder, ''Experiments on the stability of spiral flow at low axial Reynolds numbers,'' Proc. R. Soc. London, Ser. A **265**, 198 (1962).
[12] K. W. Schwarz, B. E. Springett, and R. J. Donnelly, ''Modes of instability in spiral flow between rotating cylinders,'' J. Fluid Mech. **20**, 281 (1964).
[13] R. C. Giordano, R. L. C. Giordano, D. M. F. Prazeres, and C. L. Cooney, ''Analysis of a Taylor–Poiseuille vortex flow reactor. I: Flow patterns and mass transfer characteristics,'' Chem. Eng. Sci. **53**, 3635 (1998).
[14] R. J. Donnelly and D. Fultz, ''Experiments on the stability of spiral flow between rotating cylinders,'' Proc. Natl. Acad. Sci. USA **46**, 1150 (1960).
[15] N. Gravas and B. W. Martin, ''Instability of viscous axial flow in annuli having a rotating inner cylinder,'' J. Fluid Mech. **86**, 385 (1978).
[16] M. M. Sorour and J. E. R. Coney, ''The characteristics of spiral vortex flow at high Taylor numbers,'' J. Mech. Eng. Sci. **21**, 65 (1979).
[17] K. L. Babcock, G. Ahlers, and D. S. Cannell, ''Noise-sustained structure in Taylor–Couette flow with through flow,'' Phys. Rev. Lett. **67**, 3388 (1991).
[18] A. Tsameret and V. Steinberg, ''Noise-modulated propagating pattern in a convectively unstable system,'' Phys. Rev. Lett. **67**, 3392 (1991).
[19] P. Büchel, M. Lücke, D. Roth, and R. Schmitz, ''Pattern selection in the absolutely unstable regime as a nonlinear eigenvalue problem: Taylor vortices in axial flow,'' Phys. Rev. E **53**, 4764 (1996).
[20] A. Tsameret and V. Steinberg, ''Absolute and convective instabilities and noise-sustained structures in the Couette–Taylor system with an axial flow,'' Phys. Rev. E **49**, 1291 (1994).
[21] J. Kaye and E. C. Elgar, ''Modes of adiabatic and diabatic fluid flow in an annulus with an inner rotating cylinder,'' Trans. ASME **80**, 753 (1958).
[22] K. M. Becker and J. Kaye, ''Measurements of diabatic flow in an annulus with an inner rotating cylinder,'' J. Heat Transfer **84**, 97 (1962).
[23] K. Beranek, I. Streda, and J. Sestak, ''On the flow of viscous liquids through annular clearances with the rotating inner cylinder,'' Acta Tech. CSAV **24**, 665 (1979).
[24] K. Kataoka, H. Doi, and T. Komai, ''Heat/mass transfer in Taylor vortex flow with constant axial flow rates,'' Int. J. Heat Mass Transfer **20**, 57 (1977).
[25] Z. H. Gu and T. Z. Fahidy, ''Visualization of flow patterns in axial flow between horizontal coaxial rotating cylinders,'' Can. J. Chem. Eng. **63**, 14 (1985).
[26] Z. H. Gu and T. Z. Fahidy, ''Characteristics of Taylor vortex structure in combined axial and rotating flow,'' Can. J. Chem. Eng. **63**, 710 (1985).
[27] Z. H. Gu and T. Z. Fahidy, ''The effect of geometric parameters on the structure of combined axial and Taylor-vortex flow,'' Can. J. Chem. Eng. **64**, 185 (1986).
[28] K. Bühler and N. Polifke, ''Dynamical behaviour of Taylor vortices with superimposed axial flow,'' in *Nonlinear Evolution of Spatio-Temporal Structures in Dissipative Continuous Systems*, edited by F. H. Busse and L. Kramer (Plenum, New York, 1990), Vol. Series B:Physics Vol. 225, pp. 21–29.
[29] R. M. Lueptow, A. Docter, and K. Min, ''Stability of axial flow in an annulus with a rotating inner cylinder,'' Phys. Fluids A **4**, 2446 (1992).
[30] K. N. Astill, ''Studies of the developing flow between concentric cylinders with the inner cylinder rotating,'' J. Heat Transfer **86**, 383 (1964).
[31] D. A. Simmers and J. E. R. Coney, ''The experimental determination of velocity distribution in annular flow,'' Int. J. Heat Fluid Flow **1**, 177 (1979).
[32] K. Min and R. M. Lueptow, ''Circular Couette flow with pressure-driven axial flow and a porous inner cylinder,'' Exp. Fluids **17**, 190 (1994).
[33] R. M. Lueptow and A. Hajiloo, ''Flow in a rotating membrane plasma

separator,'' Am. Soc. Artif. Int. Organs J. **41**, 182 (1995).
[34]J. Parker and P. Merati, ''An investigation of turbulent Taylor–Couette flow using laser Doppler velocimetry in a refractive index matched facility,'' J. Fluids Eng. **118**, 810 (1996).
[35]R. P. Dring, ''Sizing Criteria for Laser Anemometry Particles,'' ASME J. Fluid Eng. **104**, 15 (1982).
[36]P. R. Fenstermacher, H. L. Swinney, and J. P. Gollub, ''Dynamical instabilities and the transition to chaotic Taylor vortex flow,'' J. Fluid Mech. **94**, 103 (1979).
[37]C. D. Andereck, S. S. Liu, and H. L. Swinney, ''Flow regimes in a circular Couette system with independently rotating cylinders,'' J. Fluid Mech. **164**, 155 (1986).
[38]R. C. DiPrima and H. L. Swinney, ''Instabilities and transition in flow between concentric rotating cylinders,'' in Topics in Applied Physics, Hydrodynamic Instabilities and the Transition to Turbulence, edited by H. L. Swinney and J. P. Gollub (Springer-Verlag, Berlin, 1985), pp. 139–180.
[39]J. P. Gollub and H. L. Swinney, ''Onset of turbulence in a rotating fluid,'' Phys. Rev. Lett. **35**, 927 (1975).
[40]R. J. Donnelly, K. Park, R. Shaw, and R. W. Walden, ''Early nonperiodic transitions in Couette flow,'' Phys. Rev. Lett. **44**, 987 (1980).
[41]M. Stöckert and R. M. Lueptow, ''Velocity field in Couette Taylor flow with axial flow,'' in *10th International Couette-Taylor Workshop*, edited by C. Normand and J. E. Wesfreid (Paris, 1997), pp. 147–148.
[42]S. T. Wereley and R. M. Lueptow, ''Spatio-temporal character of supercritical circular Couette flow,'' J. Fluid Mech. **364**, 59 (1998).
[43]P. S. Marcus, ''Simulation of Taylor–Couette flow. Part 2. Numerical results for wavy-vortex flow with one travelling wave,'' J. Fluid Mech. **146**, 65 (1984).
[44]R. J. Campero and R. D. Vigil, ''Spatio-temporal patterns in liquid-liquid Taylor-Couette-Poiseille flow,'' Phys. Rev. Lett. **79**, 3897 (1997).
[45]D. Coles, ''Transition in circular Couette flow,'' J. Fluid Mech. **21**, 385 (1965).